

Article

# Imaging Arctic Permafrost: Modeling for Choice of Geophysical Methods

Igor Buddo<sup>1,2,3,\*</sup>, Natalya Misyurkeeva<sup>1,2,3</sup>, Ivan Shelokhov<sup>1,2,3</sup>, Evgeny Chuvilin<sup>4</sup>, Alexey Chernikh<sup>2</sup> and Alexander Smirnov<sup>3,5</sup>

<sup>1</sup> Institute of the Earth's Crust, Siberian Branch of the Russian Academy of Sciences, 664033 Irkutsk, Russia

<sup>2</sup> School of Subsurface Resource Management, Irkutsk National Research Technical University, 664074 Irkutsk, Russia

<sup>3</sup> Arctic Research Center of the Yamal-Nenets Autonomous District, 629008 Salekhard, Russia

<sup>4</sup> Skolkovo Institute for Science and Technology, 121205 Moscow, Russia

<sup>5</sup> Department of Applied Geophysics, Institute of Geology and Oil and Gas Production, Industrial University of Tyumen, 625000 Tyumen, Russia

\* Correspondence: biv@crust.irk.ru

**Abstract:** Knowledge of permafrost structure, with accumulations of free natural gas and gas hydrates, is indispensable for coping with spontaneous gas emission and other problems related to exploration and production drilling in Arctic petroleum provinces. The existing geophysical methods have different potentialities for imaging the permafrost base and geometry, vertical fluid conduits (permeable zones), taliks, gas pockets, and gas hydrate accumulations in the continental Arctic areas. The synthesis of data on cryological and geological conditions was the basis for a geophysical–geological model of northern West Siberia to a depth of 400 m, which includes modern permafrost, lenses of relict permafrost with hypothetical gas hydrates, and a permeable zone that may be a path for the migration of gas–water fluids. The model was used to model synthetic seismic, electrical resistivity tomography (ERT), and transient electromagnetic (TEM) data, thus testing the advantages and drawbacks of the three methods. Electrical resistivity tomography has insufficient penetration to resolve all features and can run only in the summer season. Seismic surveys have limitations in mapping fluid conduits, though they can image a horizontally layered structure in any season. Shallow transient electromagnetic (sTEM) soundings can image any type of features included into the geological model and work all year round. Thus, the best strategy is to use TEM surveys as the main method, combined with seismic and ERT data. Each specific method is chosen proceeding from economic viability and feasibility in the specific physiographic conditions of mountain and river systems.

**Keywords:** Arctic; permafrost; gas hydrates; seismic surveys; resistivity surveys; electrical resistivity tomography; transient electromagnetic soundings



**Citation:** Buddo, I.; Misyurkeeva, N.; Shelokhov, I.; Chuvilin, E.; Chernikh, A.; Smirnov, A. Imaging Arctic Permafrost: Modeling for Choice of Geophysical Methods. *Geosciences* **2022**, *12*, 389. <https://doi.org/10.3390/geosciences12100389>

Academic Editors: Christina Biasi and Jesus Martinez-Frias

Received: 23 September 2022

Accepted: 18 October 2022

Published: 21 October 2022

**Publisher's Note:** MDPI stays neutral with regard to jurisdictional claims in published maps and institutional affiliations.



**Copyright:** © 2022 by the authors. Licensee MDPI, Basel, Switzerland. This article is an open access article distributed under the terms and conditions of the Creative Commons Attribution (CC BY) license (<https://creativecommons.org/licenses/by/4.0/>).

## 1. Introduction

Permafrost in the Russian Arctic regions, including northern West Siberia, formed through the Quaternary under changing climate conditions, with intermittent cooling and warming stages, ice-sheet glaciation, and the transgression and regression of Arctic seas. Therefore, the Arctic permafrost has a layered structure and includes widespread ground ice and unfrozen (talik) zones [1]. More complexity has been the result of the lithological heterogeneity and permeability of deformed freezing sediments: neotectonic deformation of such sediments produced conduits for gaseous and aqueous fluids as a prerequisite for the formation of intra- and sub-permafrost gas hydrates.

Many gas fields in the permafrost areas of West Siberia store gas hydrates, both at the depths of hydrate stability [2,3] and in shallow permafrost, where gas hydrates formed under the pressure and temperature conditions that were favorable in the past, but are

metastable at present [4–6]. The metastable relict gas hydrates may cause an emergency, associated with gas emissions during drilling and the operation of wells in the Arctic petroleum provinces [7]. The emission of pressurized gas can be explosive and produce the craters found in northern West Siberia [8,9].

The extent and geometry of the Arctic permafrost can be imaged by geophysical surveys, in addition to direct sampling by geological and geocryological methods. The importance of geophysical surveys, as a major tool in permafrost mapping, was recognized long ago [10–14], but their application in the previous years was limited to direct current (DC) resistivity and shallow seismic surveys. Nevertheless, those data were the basis for models that image permafrost to depths of a few tens of meters [15,16].

Investigating the complex permafrost structure, with free gas and gas hydrate accumulations till depths of 500 m, is challenging. Using seismic [17–21] and resistivity (CSEM) [22–26] exploration geophysics for detecting gas pockets and gas hydrates in unfrozen rocks are rewarding experiences [27], but these methods can hardly discriminate between the permafrost and gas hydrate zones, which have similar resistivity and acoustic signatures.

Thus, it is critical to choose the optimal techniques for mapping the continental Arctic permafrost that may enclose the lenses of the relict permafrost with hypothetical gas hydrates and intricate fluid migration paths. We are testing the potentialities of seismic and resistivity surveys, in this respect, by modeling the synthetic data based on well logs and previous field results.

## 2. History of Permafrost in Northern West Siberia

The complex structure of permafrost in northern West Siberia [1] formed during the Quaternary warm and cold events [28], in four major stages (Figure 1).

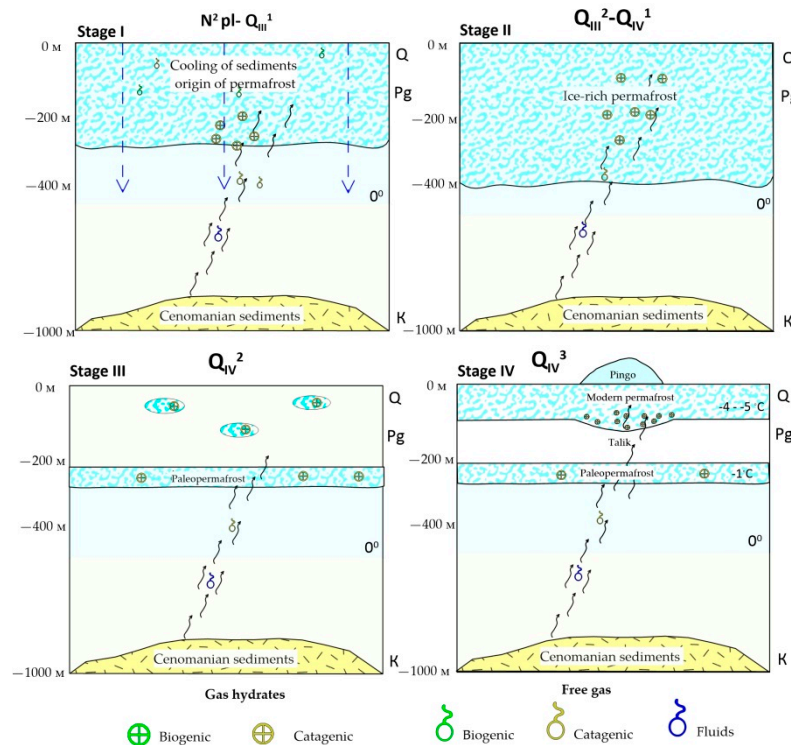


**Figure 1.** Sketch of permafrost history in northern West Siberia. Stage 1–IV–stages of permafrost formation: Stage 1–latest Pliocene (N2pl); Stage 2–Early Zyryanian (Yermakovian) cryochron (QIII2); Stage 3–mainly Middle Holocene (QIV2); Stage 4–Late Holocene to present (~3.0–4.5 kyr).

**Stage 1,** latest Pliocene (N2pl) through earliest Late Pleistocene (QIII1): prolonged cooling of sediments and permafrost origin. The Middle Pleistocene permafrost in West

Siberia was apparently as thick as 600–800 m in the north [29] and 300–400 m south of the W–E Ob River segment. Gas hydrates possibly appeared in the freezing sediments during that period [30].

**Stage 2**, Early Zyryanian (Yermakovian) cryochron ( $Q_{III}^2$ ) through Early Holocene ( $Q_{IV}^1$ ): main event of permafrost formation during the Zyryanian glacial [31,32], the last ice-sheet glaciation in the northern West Siberian Plain [33]. The permafrost thickness reached hundreds of meters, judging by the 200 m depth to the base of the relict permafrost within the region. The conditions in thick permafrost were favorable for the formation of gas hydrates over a large depth range.

**Stage 3**, mainly Middle Holocene ( $Q_{IV}^2$ ): permafrost degradation, both from above and from below, during the warming event, which culminated at 10–11 kyr BP (Holocene climate optimum) and was prominent in northern West Siberia between 9.0 kyr and 4.5 kyr BP [34]. In that period, the 400 m thick permafrost thawed from above for 100–200 m and became warmer, though still preserved, below that depth. As a result of permafrost degradation, the zone of hydrate stability moved to greater depths and gas hydrates became partly decomposed. However, some permafrost remnants may have survived in zones cooled down by the heat-consuming hydrate dissociation (complete or partial).

**Stage 4**, Late Holocene to present (~3.0–4.5 kyr): expansion of permafrost during cooling to its modern configuration. The permafrost that formed during the cooling period coalesced with the paleo permafrost in the northern areas, but penetrated to only 130–150 m, leaving the older relict permafrost as another layer below in the south. At that period, cryogenic landscapes were shaping up by surface and subsurface processes.

The climate cooling caused the freezing of gas-saturated pore fluids, which produced a growing permafrost screen. Gas, which is insoluble in ice, became expelled from pore water toward the deepening permafrost base. Thus, gas accumulation occurred throughout the sedimentary sequence [35].

The pressure and temperature in thick permafrost, both on the shore and in the shelf, correspond to the conditions of gas hydrate stability [30]. Meanwhile, the mere presence of permafrost is a necessary, but insufficient, condition for the existence of large gas hydrate accumulations, which require sufficient amounts of gas, water, and space in permeable sediments, besides the special *PT* conditions.

Permeable permafrost contains paths for gas migration, which produced pingo-like features in northern West Siberia [36,37]. The resistivity patterns of sediments beneath the pingoes were modeled [38–40], proceeding from the hypothesis that the Arctic cryogenic landforms, such as pingoes, are related to the subsurface fluid dynamic processes and can trace potential gas emission sites as indicators of degassing. The modeling revealed resistivity and seismic anomalies that recorded changes in the permafrost and highlighted the sites of pending gas emission events.

Thus, data from the northern West Siberian petroleum province provide evidence that zones of thick metastable permafrost may store gas hydrates that originated from biogenic or sediment maturation (catagenic) processes.

### 3. Geophysical–Geological Model of Northern West Siberia

The physical fields of northern West Siberia were simulated in a basic geophysical–geological model, with reference to sonic and resistivity well logs and core analysis [38,40–42]. Seismic and resistivity surveys are applicable to permafrost imaging because ice-rich rocks stand out in high seismic velocities and high resistivity [43]. Thus, distinct contrasts between frozen and unfrozen rocks allow for the mapping of permafrost-talik interfaces and, possibly, resolving gas hydrates and vertical fluid conduits [39,41]. This hypothesis was checked using a basic geological model (Figure 2), which then provided reference for further modeling.

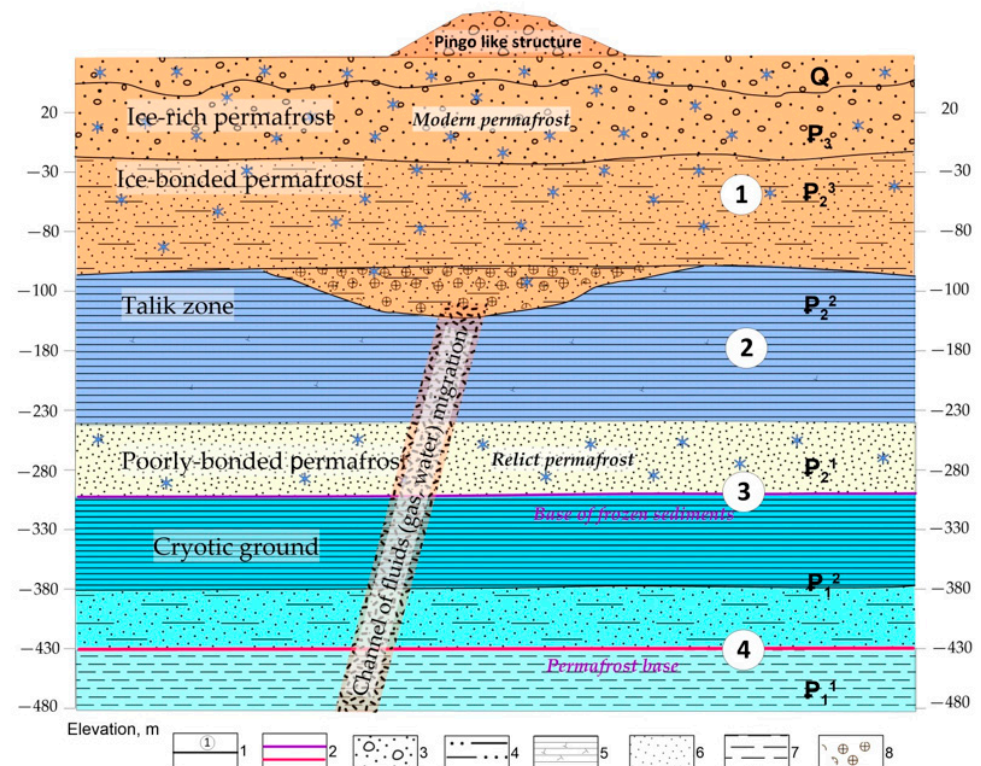


**Figure 2.** Geological model. 1 = layer numbers and boundaries; 2 = inferred boundaries of permafrost and cryotic sediments; 3 = sandy loam and loam with sand, gravel, pebble, and organic detritus intercalations; 4 = sand with clays and gravel lenses and layers; 5 = montmorillonite and diatomaceous clay with diatomite; 6 = fine kaolinized sand; 7 = diatomaceous opoka clay; 8 = gas hydrates.

The model consists of six layers (four layers of similar physical properties), with a total thickness of 480 m and a length of 5000 m. The model includes a pingo-like feature (a mound on the surface), with a thick layer of high-velocity and high-resistivity rocks underneath. The increase of permafrost thickness may be evidence of a gas hydrate accumulation in a metastable zone [40,44]. The existence of gas hydrates in the Arctic permafrost has been confirmed in many studies [2,3,6,45–47].

The resistivity pattern used in the model is based on data collected between 2017 and 2022 [38–40]. The  $P$ -wave velocities are according to sonic logs from the region (Figure 3).

Layer 1: A pingo, ice-rich, modern permafrost ( $-5\text{ }^{\circ}\text{C}$ ) and remnant lenses of paleo permafrost, possibly with gas hydrates. The modern permafrost is composed of Quaternary lacustrine-alluvial, alluvial-marine, and glacial-marine sediments. The  $P$  velocity and resistivity assumptions are, respectively, 4000 m/s and 2000 Ohm·m.

Layer 2: Taliks, within  $-0.5\text{ }^{\circ}\text{C}$ ; montmorillonite and diatomaceous clay with diatomite; low  $P$  velocity (2600 m/s) and resistivity (15 Ohm·m). The interface between layers 1 and 2 produces the strongest anomalies. The layer additionally includes lenses of paleo permafrost with gas hydrates marked by higher  $P$  velocity (3800 m/s) and resistivity (350 Ohm·m).

Layer 3: Paleo permafrost in the lower part of the Eocene-Paleocene sequence of alternating fine to medium sands and diatomaceous opoka clay ( $-2$  to  $0\text{ }^{\circ}\text{C}$ ), as well as a clay layer below. The  $P$  velocity and resistivity are, respectively, 3200 m/s and 30 Ohm·m.

Layer 4: Cryotic sediments,  $-1$  to  $0\text{ }^{\circ}\text{C}$ ; dark-grey micaceous silty clay with sand and silt layers. The  $P$  velocity and resistivity are, respectively, 3500 m/s and 20 Ohm·m.

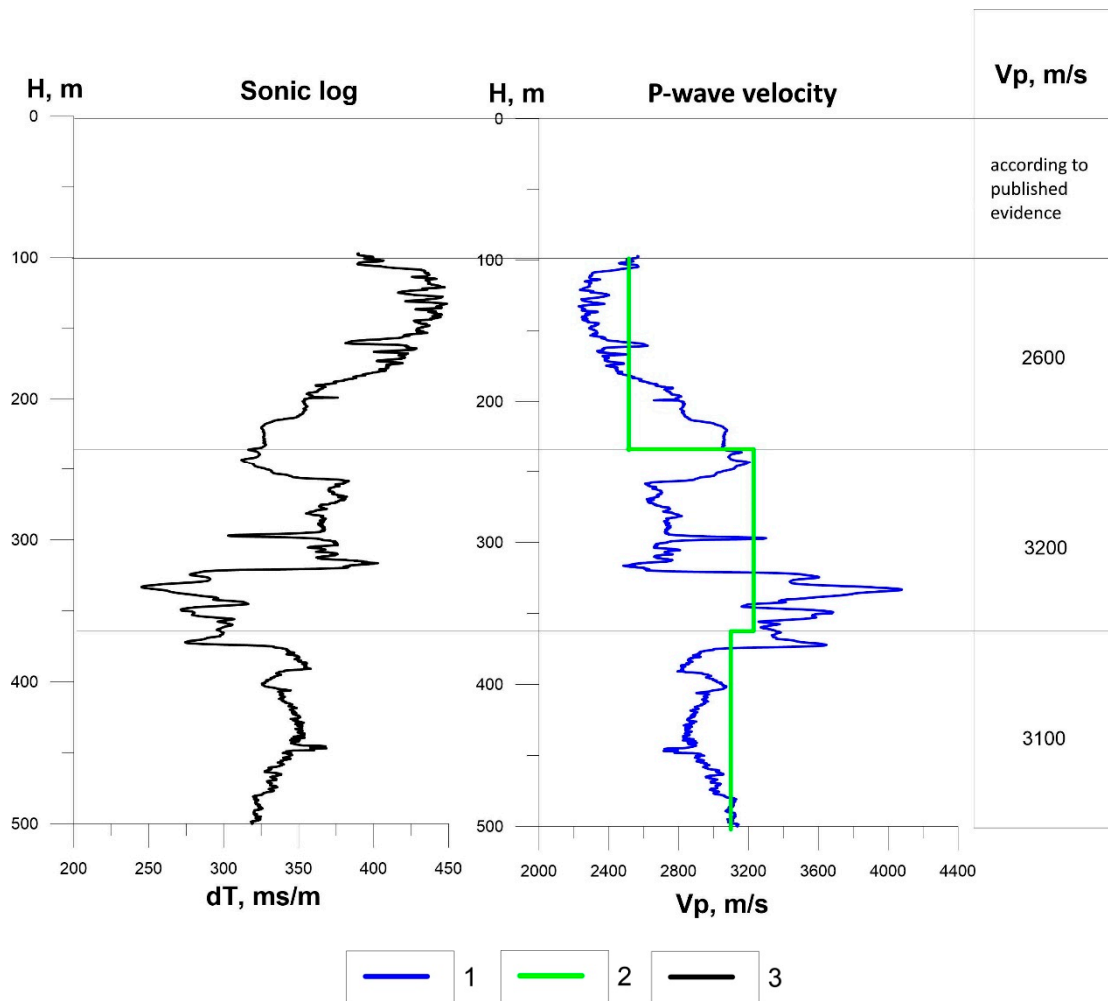


**Figure 3.** P-wave travel times and velocities used for model parameterization. 1 = P-wave velocity log; 2 = average velocity model; 3 = sonic log.

**4. Methods**

The near-surface is most often studied by seismic, radar, and DC resistivity surveys, as well as by frequency- and time-domain electromagnetic soundings [48].

Shallow engineering seismic surveys can cover a depth range from a few meters to a few hundred meters [49–51] and can image the Arctic permafrost, due to strong acoustic anomalies from interfaces, such as that between unfrozen and frozen rocks [15,16]. Shallow seismic surveys are commonly accurate to a few meters, though the resolution can be higher, if the rocks are acoustically contrasting.

Resistivity methods include vertical electric soundings (VES), modified electrical resistivity tomography (ERT), ground penetrating radar (GPR), and transient electromagnetic (TEM) soundings [52], which are applicable to a wide scope of targets. DC resistivity methods, including VES and ERT, have been used broadly for many decades [53] to measure the electric field on the surface controlled by subsurface resistivity [54,55]. DC methods allow mapping resistivity layers of a few meters thick, provided that the resistivity contrast is sufficient.

Ground penetrating radar (GPR) data are responses of shallow earth to the induced electromagnetic field at frequencies from 50 to 2000 MHz [56,57]. In the Arctic conditions, GPR can image the permafrost top, as well as faults and other permeable zones [58]. However, the penetration is insufficient to reach the permafrost base, and it becomes further reduced in clayey sediments, where the radar signals attenuate rapidly. ERT

requires grounding (galvanic contact with the earth) and can be less efficient because of the screening effect from high-resistivity layers, e.g., permafrost [39,59].

TEM soundings yield transient responses of the earth (decaying voltage) to control turn-off of pulse transmitter current [60–62]. The physical background of the method, acquisition systems, and approaches to data processing and interpretation received a lot of literature, e.g., [63–67]. The use of a controlled source and ungrounded square loops ensures higher resolution and better signal-to-noise ratio, relative to the data from natural electromagnetic fields. TEM signals propagate by induction and can cover large depths, irrespective of array geometry (cable length), due to the skin effect. TEM soundings are applicable to highly resistive rocks, including frozen ground [68,69]. Inversion of TEM signals yields high-resolution models of shallow sediments, with layers thicknesses from 5 m to tens of meters at depths of 300–400 m.

TEM soundings with various advanced systems can penetrate to 500 m [38,39,41,44,70]. Ungrounded loops are advantageous in permafrost conditions and permit running the surveys in any season. For details of the methods and instruments see, e.g., [59].

In this study, we have obtained images of permafrost in northern West Siberia to a depth of 500 m by processing synthetic data with three methods:

1. Common mid-point seismic reflection profiling (CMP);
2. DC electrical resistivity tomography (ERT);
3. Shallow transient electromagnetic sounding (sTEM).

GPR data, which are limited to the upper 10 m of the near-surface, are inapplicable in our case and remain beyond the present consideration.

The CMP data were processed using the Tesseral Pro software for full-wave modeling (Tesseral Technologies Inc., Calgary, province of Alberta, Canada). Elastic waves were excited by a shot source; a 100 Hz Ricker wavelet, within a 200 Hz bandwidth, was used as a probing pulse. This frequency was chosen to achieve a resolution sufficient to image local anomalies associated with fluid conduits and gas hydrate accumulations. The vertical resolution was calculated using the Widess equation:

$$R_v = \lambda/4; \quad (1)$$

$$\lambda = V/f, \quad (2)$$

where  $R_v$  is the vertical size of the target;  $\lambda$  is the wavelength;  $V$  is the seismic velocity;  $f$  is the predominant pulse frequency. According to this equation, the vertical resolution at 100 Hz is about 10 m in the given geological conditions, which is enough for detecting local features.

The signals were from a symmetrical 48-channel system with 8 m receiver spacing, chosen as a trade-off between the lateral resolution and computing time required for each iteration in the modeling. The maximum record length was 350 ms at a stepsize of 0.2 ms, which provided a depth coverage of 500 m. The total profile length was 5000 m.

The system for ERT data was of dipole–dipole configuration, with a cable length of 1280 m, a total profile length of 5400 m, and an electrode spacing of 20 m; the data were processed in ZondRes2D [71].

The TEM data represent a 5000 m long profile, collected with a system of square ungrounded loops: a 100 m × 100 m transmitter and a 10 m × 10 m receiver, offsets from zero to 100 m, and a station spacing of 100 m. The transmitter pulse duration was 0.02 s, and the cutoff was specified at  $7 \times 10^{-6}$  s. The data were processed using software for 1D TEM modeling [72].

The modeling aimed at testing the potentialities of the methods for imaging (i) the base of ice-rich permafrost; (ii) the base of interval with lenses of paleo permafrost and hypothetical gas hydrates; and (iii) steep to vertical fluid conduits.

### 5. Results

The processing of the generated CMP, ERT, and sTEM data led to the following results, considered separately below.

#### 5.1. CMP Seismic Data

The wave patterns were modeled with reference to the starting velocity model (Figure 4), implying a high (35%) velocity difference between layers 1 and 2 and a minor (5%) difference between layers 1 and 3, which hardly would show up in the seismic images. The steep conduit stands out against the host rocks, with up to 100% *P*-wave velocity contrasts, though steep faults are hard to map from CMP reflections. Thus, the reference velocity model looks quite favorable for mapping permafrost in northern West Siberia.

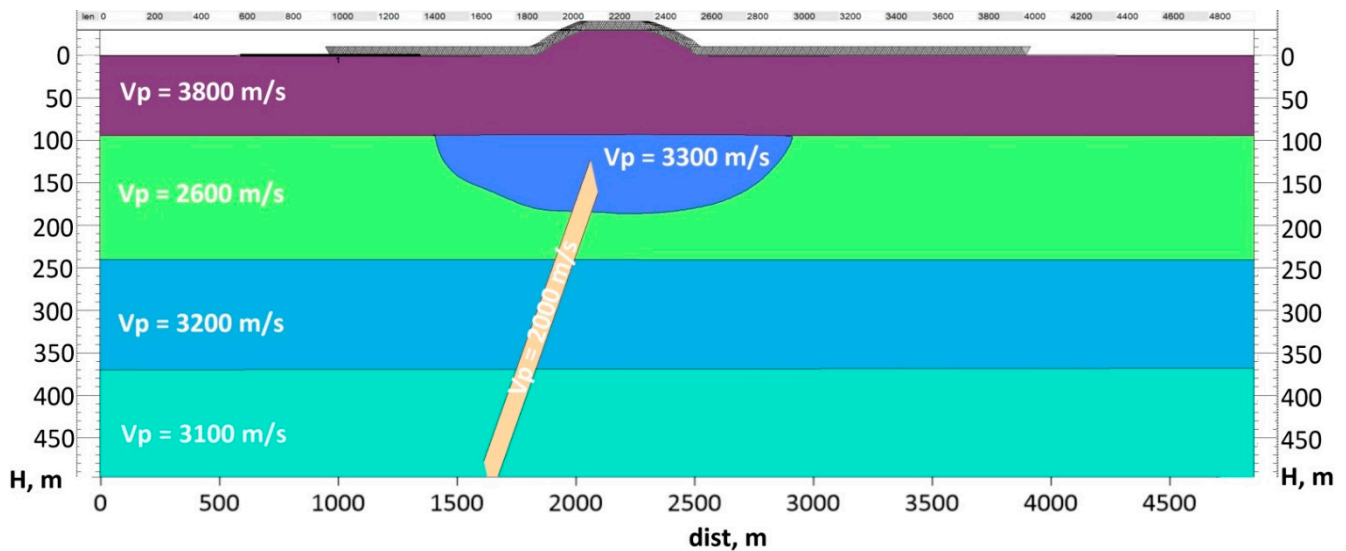


Figure 4. Starting velocity model for seismic data modeling.

The performed seismic modeling yielded an intricate wave pattern (Figure 5), with multiple reflections from the interfaces.

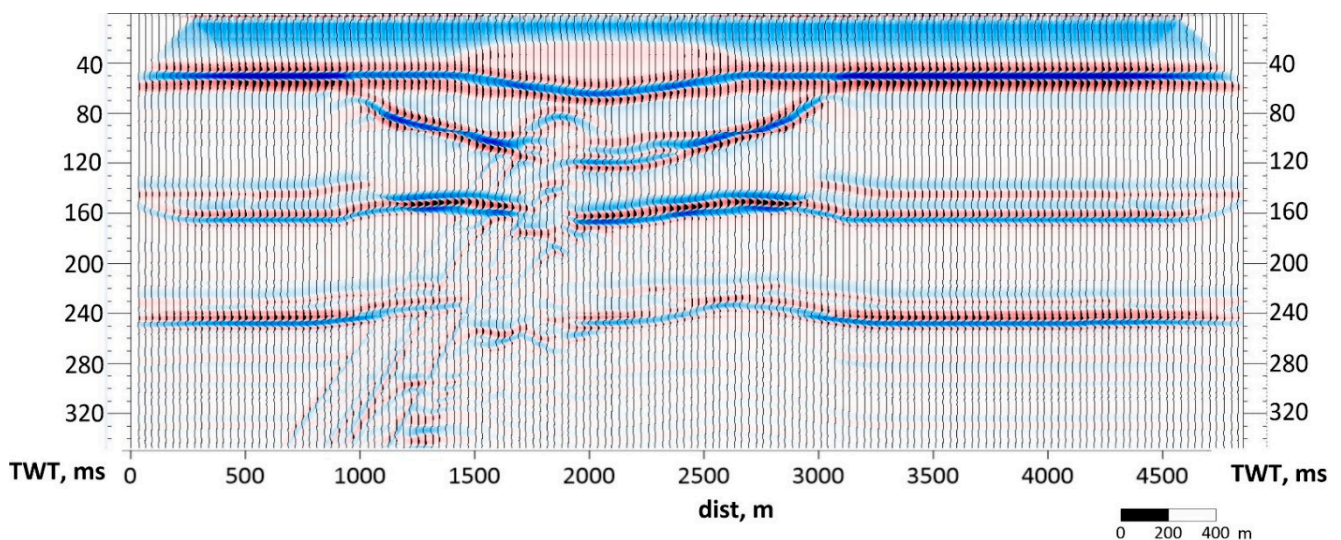


Figure 5. Synthetic CMP seismogram.

The  $V_P$  variations highlight, quite distinctly, the permafrost base and layer boundaries, as well as the base of the layer, with lenses of paleo permafrost and hypothetical gas hydrate

accumulations. The high-velocity anomaly in the central profile segment, at times, until 40 ms, with a deeper permafrost base, may be due to the presence of a pingo. The steep fluid conduit interferes with the reflection event and disturbs the wave pattern, along with ghost waves. The data allow for detecting the permeable zone, if not the conduit itself.

5.2. ERT Data

The electrical resistivity tomography (ERT) data were processed to obtain an apparent resistivity pattern using a starting model (Figure 6) on a 10 × 10 m grid, with high-resistivity layer 1 (2000 Ohm·m). The layer thickens up on account of a 350 Ohm·m local zone, which may accommodate gas hydrates and stand out against low-resistivity (15 Ohm·m) layer 2. Therefore, the boundary between layers 1 and 2 must be well-resolvable by DC resistivity methods. The 30 Ohm·m layer 3 is easy to discriminate from the sediments above and below. The fluid conduit is a permeable zone, with resistivity as low as 15 Ohm·m.

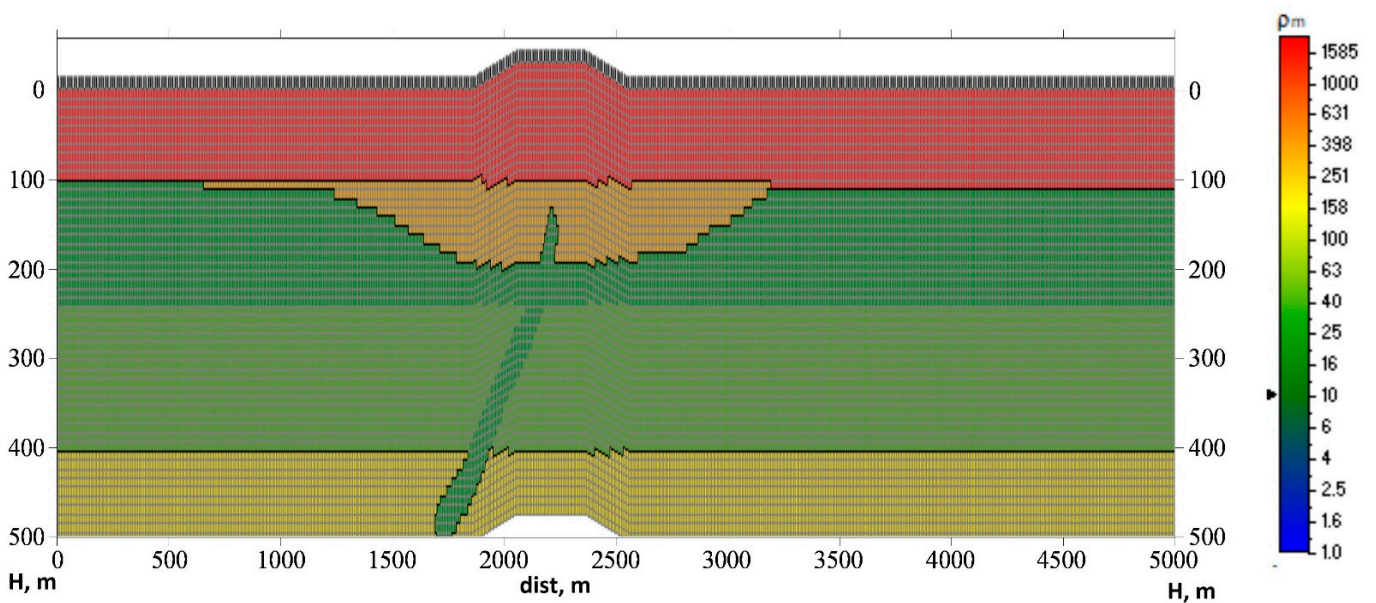


Figure 6. Starting model for ERT modeling.

Thus, the permafrost intervals of different thicknesses, with hypothetical gas hydrates and paleo permafrost, have higher resistivity than cryotic and unfrozen rocks. The inversion of ERT data yielded a pattern with smoothly changing resistivity (Figure 7).

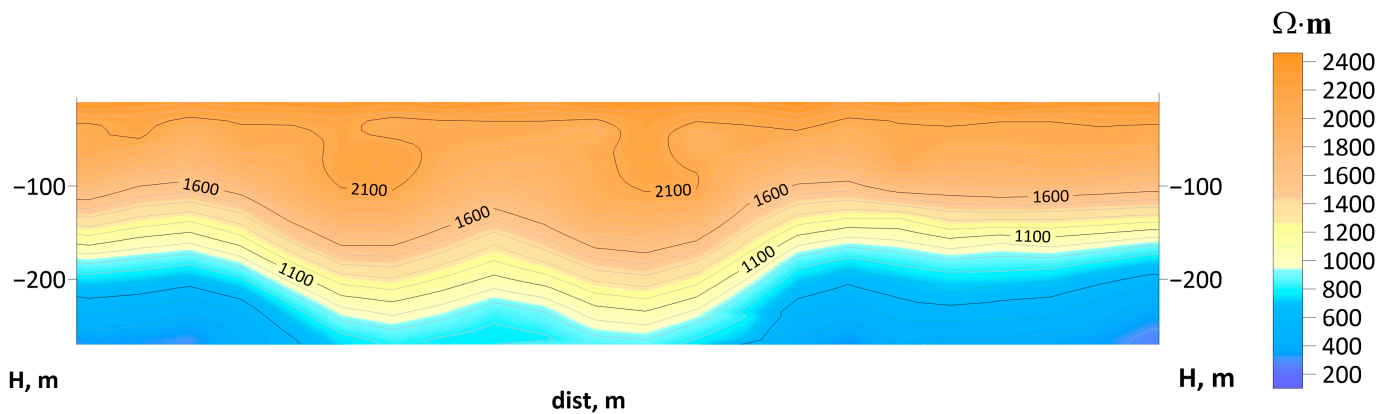


Figure 7. Apparent resistivity cross-section obtained from ERT data.

Since the transitions are very smooth, the interface between frozen and unfrozen sediments is traceable only from the resistivity gradient. High-resistivity rocks in the

central segment of the profile are thicker, due to the effect of paleo permafrost lenses with hypothetical gas hydrates. The conductor, possibly associated with a fluid conduit, divides the high-resistivity zone into halves, but the conduit itself remains unresolved. Note that the cable length (1280 m) provides penetration within only 200–250 m, according to the geometry of the DC soundings.

5.3. TEM Data

The starting model for obtaining an apparent resistivity pattern from transient responses (Figure 8) had parameters similar to those in the model for ERT, with a lateral grid spacing of 100 m.

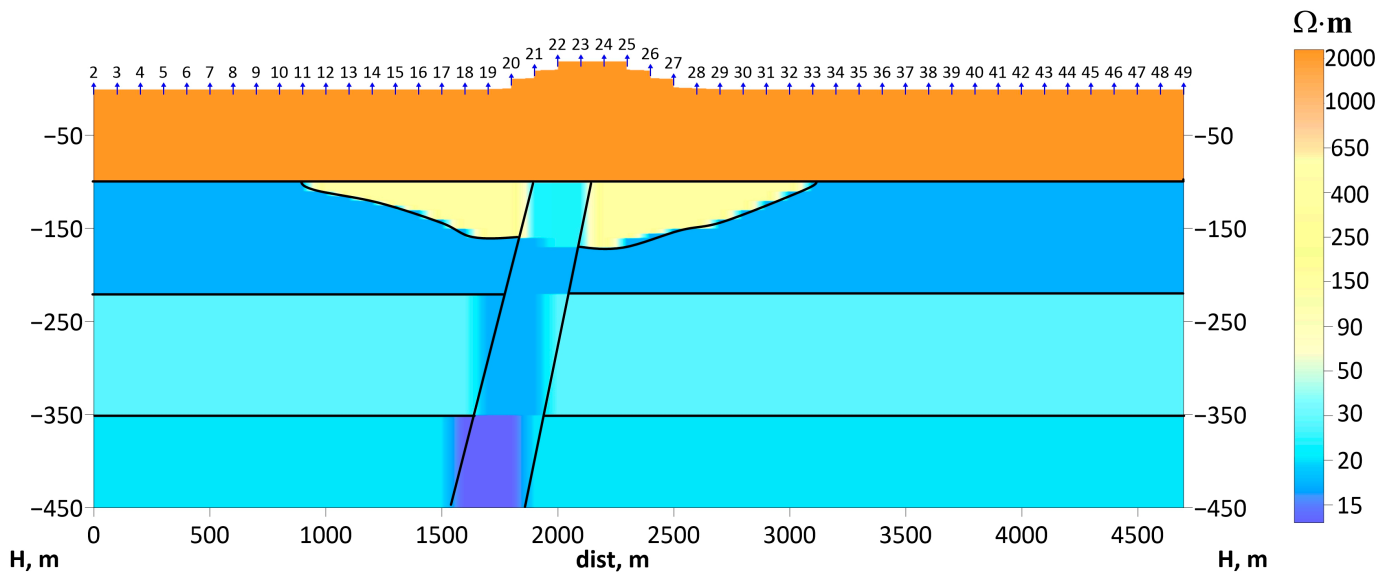


Figure 8. Starting model for TEM modeling.

The imaging results, based on TEM data, are shown in Figure 9.

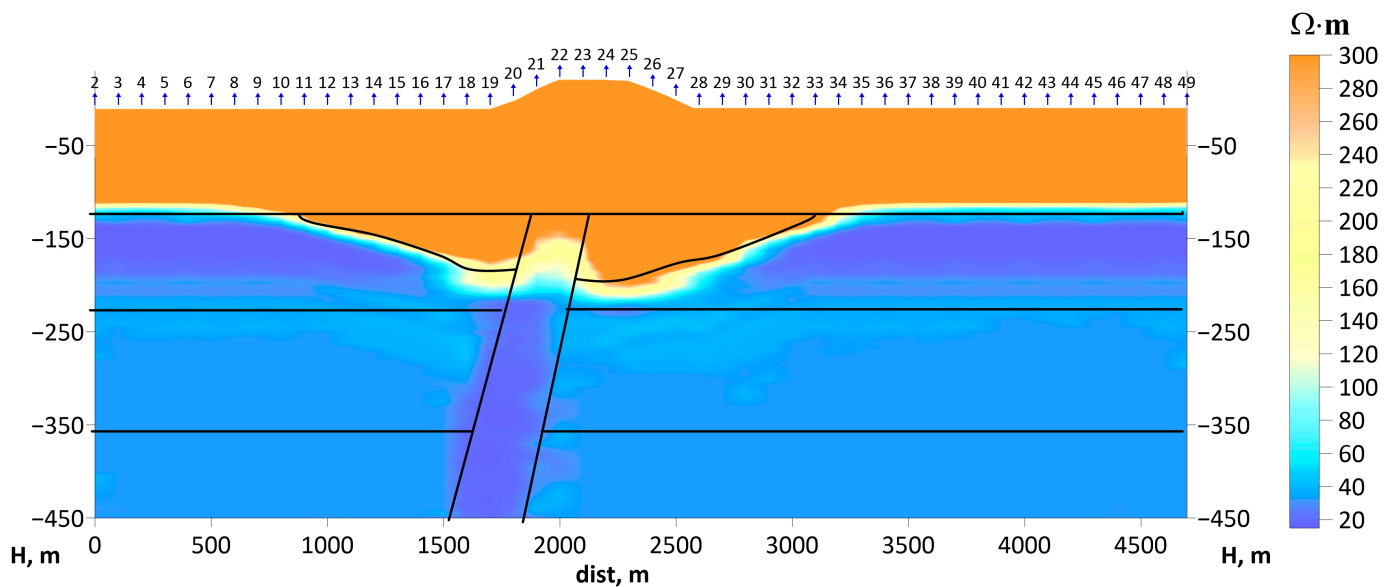
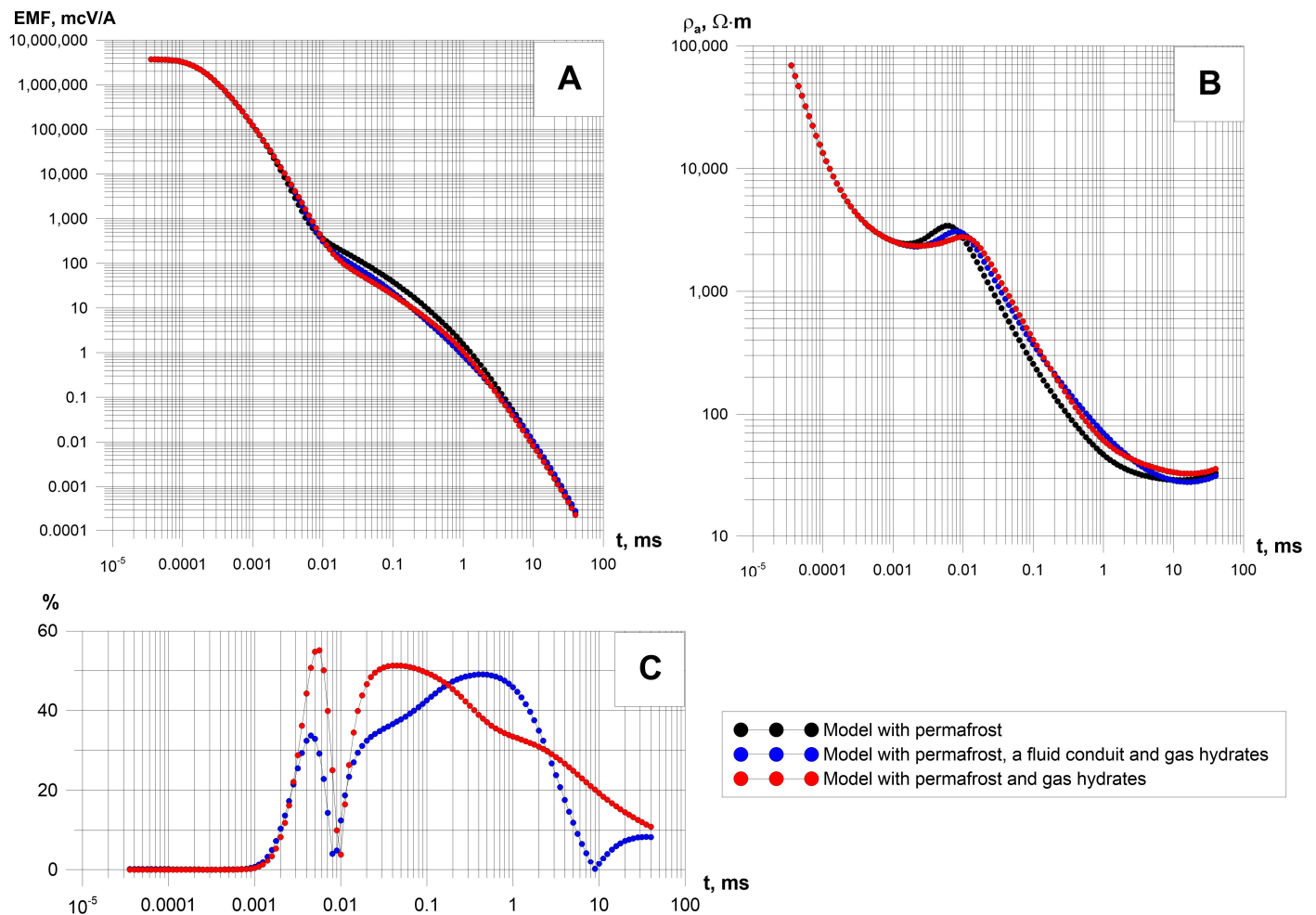


Figure 9. Apparent resistivity cross-section obtained from TEM data.

The resistivity cross-section perfectly reproduces the boundary between ice-rich layer 1 and the talik, but the boundary of thickened permafrost, with hypothetically enclosed gas hydrates, is less prominent, except for a small gradient zone of medium resistivity

(100–200 Ohm·m). The reason is that the TEM method has low sensitivity to high-resistivity targets: it is almost impossible to discriminate between 300 Ohm·m and 2000 Ohm·m rocks in TEM curves. The boundaries between layers 2, 3, and 4 are almost mute in the apparent resistivity pattern because the resistivity difference is small. Meanwhile, the steep conduit shows up distinctly, i.e., TEM surveys can detect such features quite well.

Figure 10 shows the synthetic curves generated from the TEM data.



**Figure 10.** Synthetic TEM curves: voltage (emf) decay (A), apparent resistivity (B), and EMF anomaly (C), relative to the reference model with permafrost.

The curves corresponding to the background conditions (station 5) represent permafrost of a stable thickness without a fluid conduit. The responses from station 25 show local permafrost thickening with hypothetical gas hydrates, but no fluid conduit; the latter is evident in the data from station 20, which are otherwise similar to station 25.

The TEM curves differ markedly, depending on conditions, e.g., the anomaly, relative to the background setting, exceeds 50% (Figure 9). Note that the effect from gas hydrates appears in a 0.01–0.5 ms interval, while the conduit shows up at later times (0.1–1.0 ms). Thus, all these features can be reliably imaged by TEM soundings (Figure 11), as it was shown in our recent paper [41].

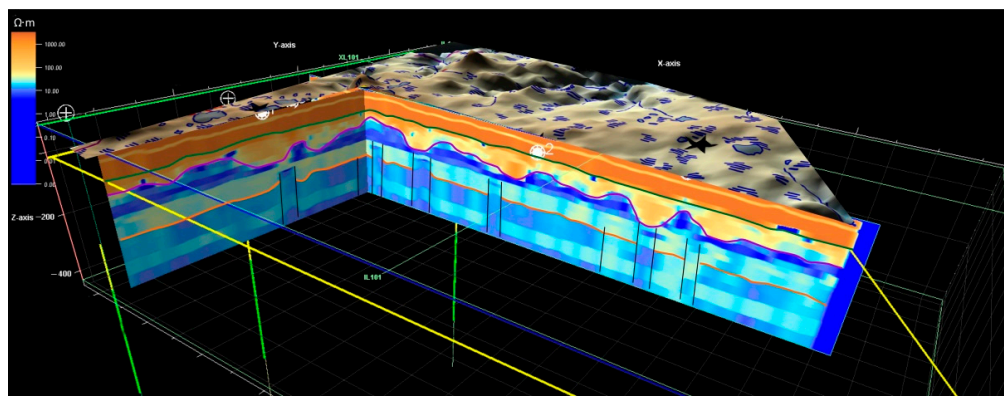


**Figure 11.** Example resistivity model of shallow subsurface, based on sTEM data [41].

## 6. Discussion

The modeling and field results allow some inferences on the potentialities of different geophysical methods, as to the mapping of the permafrost base and possible changes in its geometry in the presence of paleo permafrost or gas hydrate accumulations. Shallow CMP seismic profiling provides reliable images of the near surface, provided that the layers have contrasting acoustic properties. However, the wave pattern can be distorted by various features in permafrost, which interfere with data processing and the interpretation of the results. Steep to vertical interfaces, especially fluid conduits, are hard to identify in CMP data.

DC resistivity methods (VES and ERT) are broadly used in northern West Siberia, due to the simplicity of acquisition and processing. They are efficient in imaging the upper 30–50 m of the section, but are of low performance for depths below 100 m, which makes these methods poorly applicable to the mapping of permafrost that may reach hundreds of meters thick. Penetration to 500–600 m requires cable lengths of at least 3000 m, which is unreasonable. Moreover, the surveys are unfeasible in the winter season in the Arctic conditions, as the source and receiver units have to be grounded.

In this respect, TEM surveys are advantageous for imaging the Arctic permafrost. Indeed, the induction principle of field propagation and the dependence of the penetration (skin) depth on the duration of the transient process and on the resistivity allow for seeing depths below 500 m, even with small loops [59]. Furthermore, the surveys with ungrounded transmitter and receiver loops can be run in any season irrespective of the frost depth and temperature. According to the modeling results, the TEM method resolves well the permafrost base, the paleo permafrost lenses with hypothetical gas hydrates, and the steep fluid conduits, which were reported from the field campaigns, as well [38–40,59,73,74].

The three methods are compared in Table 1.

**Table 1.** Different geophysical methods for mapping Arctic permafrost.

Method	Base of Ice-Rich Permafrost	Base of Relict Permafrost Lenses with Hypothetical Gas Hydrates	Vertical Fluid Conduits
CMP	+	+	–
ERT	+	–	–
TEM	+	+	+

Further work to develop the suggested approaches and to corroborate the existence of the inferred anomalies may consist of field experiments, checking the modeling results against well logs, and the joint inversion and interpretation of geological and geophysical data.

## 7. Conclusions

The Arctic permafrost, with frozen and unfrozen rocks, lenses of paleo permafrost that may enclose gas hydrates, and steep permeable zones as possible conduits of gaseous and aqueous fluids, can be modeled using different geophysical data.

The permafrost of northern West Siberia has had a complex history. Gases released in the course of sediment maturation or microbial metabolism migrated along permeable zones (steep to vertical conduits) and possibly induced the formation of gas hydrates and pingoes. The fluid conduits, zones of thick permafrost, and pingoes were detected during geophysical surveys in the region and were included in a geophysical–geological model, which was used for reference in further modeling of synthetic seismic and resistivity data.

The modeling results demonstrated that geological targets in the Arctic permafrost areas can be better revealed by seismic and, especially, transient electromagnetic surveys. The sTEM data highlight all three types of features, while DS resistivity and GPR methods have limited penetration. Seismic reflection profiling can be used jointly with other methods, mainly for mapping a horizontally layered earth. Thus, TEM soundings can be considered as the leading method for permafrost mapping to a depth of 500 m.

The modeling results are consistent with the field data from northern West Siberia. The high performance and economic viability of the TEM method were demonstrated earlier in the permafrost studies. High-density sTEM surveys are currently used for exploration in the Yamal Peninsula, where they cover more than 4000 km<sup>2</sup>.

The reported results have implications for the optimal ways for geophysical investigation of the Arctic permafrost, with regard to climate, river networks, and surface topography. The best strategy is to use sTEM surveys as the leading method, combined with the methods of seismic profiling (any season) and ERT (only summer). The geophysical data can additionally be checked against well logs and laboratory modeling, which will improve the quality of the final inferences, due to the more precise linkage of geophysical and geological features.

**Author Contributions:** I.B.: problem formulation, physical background, methods, data analysis, discussion, and conclusions; I.S.: resistivity models, TEM signals, and seismic data modeling; N.M.: geological models of permafrost; A.C.: ERT signals modeling; E.C.: assumptions on gas hydrates origin; A.S.: editing of the manuscript. All authors have read and agreed to the published version of the manuscript.

**Funding:** The study was funded by grant 22-17-20009 from the Russian Science Foundation (<https://rscf.ru/project/22-17-20009/>, accessed on 20 September 2022). The study, 22-17-20009, was supported by the government of the Yamal-Nenets Autonomous District).

**Data Availability Statement:** The data presented in this study are available in this article. Authors included all relevant data to support the findings of this study. Other formats of this data are available on request from the corresponding author.

**Acknowledgments:** We wish to thank Yuri Agafonov, Director General of *Sigma-Geo*, for the support and useful advice. The work was conducted using equipment and infrastructure of the Centre for Geodynamics and Geochronology at the Institute of the Earth's Crust, Siberian Branch of the Russian academy of Sciences.

**Conflicts of Interest:** The authors declare no conflict of interest.

## References

1. Ershov, E.D. *Geocryology of the USSR Territory*; West Siberia, Nedra: Moscow, Russia, 1989; p. 454. (In Russian)
2. Yakushev, B.C.; Perlova, E.V.; Makhonina, N.A.; Chuvilin, E.M.; Kozlova, E.V. Gas hydrates in sediments of continents and islands. *Russ. Khimicheskii Zhurnal* **2003**, *3*, 80–90.
3. Yakushev, V.S. *Natural Gas and Gas Hydrates in Permafrost*; VNIIGAZ: Moscow, Russia, 2009; p. 192. (In Russian)
4. Chuvilin, E.M.; Guryeva, M. Experimental Study of the Self-Preservation Effect of Gas Hydrates in Frozen Sediments. In Proceedings of the 9th International Conference on Permafrost, Fairbanks, Alaska, 29 June–3 July 2008; University of Alaska: Fairbanks, AK, USA, 2008; pp. 263–267.

5. Chuvilin, E.M.; Buhanov, B.; Davletshina, D.; Grebenkin, S. Dissociation and self-preservation of gas hydrates in permafrost. *Geosciences* **2018**, *8*, 431. [[CrossRef](#)]
6. Yakushev, V.S.; Chuvilin, E.M. Natural gas and hydrate accumulation within permafrost in Russia. *Cold Reg. Sci. Technol.* **2000**, *31*, 189–197. [[CrossRef](#)]
7. Kraev, G.; Rivkina, E.; Vishnivetskaya, T.; Belonosov, A.; van Huissteden, J.; Kholodov, A.; Smirnov, A.; Kudryavtsev, A.; Teshebaeva, K.; Zamolodchikov, D. Methane in gas shows from boreholes in epigenetic permafrost of Siberian Arctic. *Geosciences* **2019**, *9*, 67. [[CrossRef](#)]
8. Chuvilin, E.; Ekimova, V.; Davletshina, D.; Sokolova, N.; Bukhanov, B. Evidence of gas emissions from permafrost in the Russian Arctic. *Geosciences* **2020**, *10*, 383. [[CrossRef](#)]
9. Chuvilin, E.; Sokolova, N.; Davletshina, D.; Bukhanov, B.; Stanilovskaya, J.; Badetz, C.; Spasennykh, M. Conceptual models of gas accumulation in the shallow permafrost of northern West Siberia and conditions for explosive gas emissions. *Geosciences* **2020**, *10*, 195. [[CrossRef](#)]
10. Dostovalov, B.N.; Kudryavtsev, V.A. *General Geocryology*; Moscow University Press: Moscow, Russia, 1967; p. 443. (In Russian)
11. Boikov, S.A. *Resistivity Survey for Engineering Geological and Geocryological Studies of Discontinuous Permafrost*; Author's Abstract, Candidate Thesis (Geology & Mineralogy); Gosstro SSSR: Moscow, Russia, 1973; p. 32. (in Russian)
12. Bogolyubov, A.N.; Bogolyubova, N.P.; Lisitsyn, V.V.; Kurandin, N.P. *Guidelines to Engineering Geophysical (Resistivity) Surveys for Construction*; Stroiizdat: Moscow, Russia, 1984; p. 104. (In Russian)
13. Zykov, Y.D. *Geophysical Methods for Permafrost Studies*; Moscow University Press: Moscow, Russia, 1999; p. 243. (In Russian)
14. Yakupov, V.S. *Geophysics of Permafrost Regions*; Yakutsk University: Yakutsk, Russia, 2008; p. 341. (In Russian)
15. Melnikov, V.P.; Skvortsov, A.G.; Malkova, G.V.; Drozdov, D.S.; Ponomareva, O.E.; Sadurtdinov, M.R.; Tsarev, A.M.; Dubrovin, V.A. Seismic studies of frozen ground in Arctic areas. *Russ. Geol. Geophys.* **2010**, *51*, 136–142. [[CrossRef](#)]
16. Skvortsov, A.G.; Tsarev, A.M.; Sadurtdinov, M.R. Seismic studies of frozen ground. *Earth's Cryosphere* **2011**, *4*, 96–98.
17. Clairmont, R.; Bedle, H.; Marfurt, K.; Wang, Y. Seismic attribute analyses and attenuation applications for detecting gas hydrate presence. *Geosciences* **2021**, *11*, 450. [[CrossRef](#)]
18. Tayber, Z.; Meilijson, A.; Ben-Avraham, Z.; Makovsky, Y. Methane hydrate stability and potential resource in the Levant Basin, southeastern Mediterranean Sea. *Geosciences* **2019**, *9*, 306. [[CrossRef](#)]
19. Lenz, B.L.; Sawyer, D.E.; Phrampus, B.; Davenport, K.; Long, A. Seismic imaging of seafloor deformation induced by impact from large submarine landslide blocks, offshore Oregon. *Geosciences* **2019**, *9*, 10. [[CrossRef](#)]
20. Bogoyavlensky, V.; Kishankov, A.; Yanchevskaya, A.; Bogoyavlensky, I. Forecast of gas hydrates distribution zones in the Arctic Ocean and adjacent offshore areas. *Geosciences* **2018**, *8*, 453. [[CrossRef](#)]
21. Ostanin, I.; Anka, Z.; Di Primio, R. Role of faults in hydrocarbon leakage in the Hammerfest Basin, SW Barents Sea: Insights from seismic data and numerical modelling. *Geosciences* **2017**, *7*, 28. [[CrossRef](#)]
22. Weitemeyer, K.A.; Constable, S.; Tréhu, A.M. A marine electromagnetic survey to detect gas hydrate at Hydrate Ridge, Oregon. *Geophys. J. Int.* **2011**, *187*, 45–62. [[CrossRef](#)]
23. Hsu, S.-K.; Chiang, C.-W.; Evans, R.; Chen, C.-S.; Chiu, S.-D.; Wang, Y.; Chen, S.-C.; Tsai, C.-H.; Lin, S.-S. Marine controlled-source electromagnetic method used for the gas hydrate investigation in the offshore area of SW Taiwan. *J. Asian Earth Sci.* **2014**, *92*, 224–232. [[CrossRef](#)]
24. Li, G.; Tang, F.; Li, C.; Lei, W.; Liu, Y. Improved detectivity for detecting gas hydrates using the weighted differential fields of the marine controlled-source electromagnetic data. *J. Mar. Sci. Eng.* **2022**, *10*, 161. [[CrossRef](#)]
25. Jing, J.; Chen, K.; Deng, M.; Zhao, Q.X.; Luo, X.H.; Tu, G.-H.; Wang, M. A marine controlled-source electromagnetic survey to detect gas hydrates in the Qiongdongnan Basin, South China Sea. *J. Asian Earth Sci.* **2019**, *171*, 201–212, ISSN 1367-9120. [[CrossRef](#)]
26. Wang, L.; Li, Y. Field Result of Marine Controlled-Source Electromagnetic Survey for Gas Hydrates in Northern South China Sea. In Proceedings of the 5th International Conference on Systems and Informatics (ICSAI), Nanjing, China, 10–12 November 2018; pp. 871–877. [[CrossRef](#)]
27. Riedel, M.; Willoughby, E.C.; Chopra, S. (Eds.) *Geophysical Characterization of Gas Hydrates, Geophysical Developments 1*; Society of Exploration Geophysicists: Sidney, BC, Canada, 2010; p. 412. [[CrossRef](#)]
28. Shpolyanskaya, N.A. Physiography of West Siberia. In *Permafrost in West Siberia: History and Distribution Patterns*; Moscow State University: Moscow, Russia, 1971; pp. 120–123. (In Russian)
29. Baulin, Y.I. *Permafrost in Petroleum Provinces of the USSR*; Nauka: Moscow, Russia, 1985; p. 176. (In Russian)
30. Drushchits, V.A.; Sadchikova, T.A.; Skolotneva, T.S. Onshore and Arctic shelf gas hydrates and Quaternary global change. *Comm. Quat.* **2011**, *71*, 124–134.
31. Saks, V.N. *The Quaternary History of the Soviet Arctic*; Glavsevmorput: Moscow-Leningrad, Russia, 1948; p. 201. (In Russian)
32. Saks, V.N. *The Quaternary Period in the Soviet Arctic*; NIIGA Transactions: Moscow, Leningrad, Russia, 1953; Volume 77, p. 627. (In Russian)
33. Arkhipov, S.A.; Astakhov, V.I.; Volkov, I.A.; Volkova, V.S.; Panychev, V.A. *Paleogeography of the West Siberian Plain in the Late Zyryanian Glacial Maximum*; Nauka: Novosibirsk, Russia, 1980; p. 114. (In Russian)
34. Vasilchuk, Y.K. Late Pleistocene and Holocene paleoclimates: Reconstructions from isotope data for ground ice and waters in permafrost regions. *Vodn. Resur.* **1990**, *6*, 162–170.

35. Cleimenov, V.F.; Kachalov, Y.M. Subpermafrost gas accumulations in the Arctic petroleum province: Mapping methodology. In *Petroleum Geology and Exploration Lines*; VNIGNI: Moscow, Russia, 2003; pp. 191–202. (In Russian)
36. Nezhdanov, A.A.; Novopashin, V.F.; Ogibenin, V.V. Mud volcanism in the north of Western Siberia. In *TyumenNIIgiprogaz*; Flat: Tyumen, Russia, 2011; pp. 74–79. (In Russian)
37. Nezhdanov, A.A.; Smirnov, A.S. (Eds.) *Fluid Dynamic Interpretation of Seismic Data: Student's Manual*; TIU: Tyumen, Russia, 2021; p. 286. (In Russian)
38. Buddo, I.V.; Misurkeeva, N.V.; Shelokhov, I.A.; Agafonov, Y.A.; Smirnov, A.S.; Zharikov, M.G.; Kulinchenko, A.S. Experience of 3D Transient Electromagnetics Application for Shallow and Hydrocarbon Exploration within Western Siberia. In Proceedings of the 79th EAGE Conference & Exhibition 2017, Paris, France, 12–15 June 2017. [[CrossRef](#)]
39. Misyurkeeva, N.; Buddo, I.; Kraev, G.; Smirnov, A.; Nezhdanov, A.; Shelokhov, I.; Kurchatova, A.; Belonosov, A. Periglacial Landforms and Fluid Dynamics in the Permafrost Domain: A Case from the Taz Peninsula, West Siberia. *Energies* **2022**, *15*, 2794. [[CrossRef](#)]
40. Misyurkeeva, N.V.; Buddo, I.V.; Agafonov, Y.A.; Smirnov, A.S.; Zharikov, M.G.; Kulinchenko, A.S. 3D TEM and sTEM results from Arctic West Siberia. In Proceedings of the Geomodel 2017, Gelendzhik, Russia, 11–14 September 2017.
41. Misyurkeeva, N.; Buddo, I.; Shelokhov, I.; Smirnov, A.; Nezhdanov, A.; Agafonov, Y. The structure of permafrost in northern West Siberia: Geophysical evidence. *Energies* **2022**, *15*, 2847. [[CrossRef](#)]
42. Misurkeeva, N.V.; Buddo, I.V.; Smirnov, A.S.; Shelokhov, I.A. Shallow transient electromagnetic method application to study the Yamal Peninsula Permafrost Zone. In Proceedings of the Geomodel 2020, Gelendzhik, Russia, 7–11 September 2020; pp. 1–6.
43. Shelokhov, I.A. *Integration of Geophysical Methods for Predicting the Near-Surface Velocity Structure*; Author's Abstract, Candidate Thesis; Institute of the Earth's Crust: Irkutsk, Russia, 2022; p. 16. (In Russian)
44. Murzina, E.V.; Pospeev, A.V.; Buddo, I.V.; Sharlov, M.V.; Seminskiy, I.K.; Misyurkeeva, N.V.; Shelokhov, I.A. Capabilities of shallow-depth transient electromagnetic soundings for identification of gas-hydrate accumulations in the cryolithozone of the northern regions of Western Siberia. *Earth's Cryosphere* **2022**, *26*, 51–62. [[CrossRef](#)]
45. Chuvilin, E.M.; Perlova, E.V.; Baranov, Y.B.; Kondakov, V.V.; Osokin, A.B.; Yakushev, V.S. *Structure and Properties of Permafrost in the Offshore Southern Bovanenkovskoye Gas Condensate Field*; GEOS: Moscow, Russia, 2007; pp. 74–113. (In Russian)
46. Chuvilin, E.M.; Davletshina, D.A.; Lupachik, M.V. Hydrate formation in frozen and thawing methane-saturated sediments. *Earth's Cryosphere* **2019**, *2*, 50–61. [[CrossRef](#)]
47. Leonov, S.A. *Prospects for the Hydration Potential of the Supra-Cenomanian Deposits in Northern West Siberia*; Author's Abstract, Candidate Thesis (Geology & Mineralogy); Gazprom VNIIGAZ: Moscow, Russia, 2010; p. 24. (In Russian)
48. Butler, D.K. (Ed.) *Near-Surface Geophysics*; SEG: Tulsa, OK, USA, 2005; p. 732.
49. Yilmaz, O. *Engineering Seismology*; SEG: Tulsa, OK, USA, 2015; p. 954.
50. Yilmaz, O. *Seismic Data Processing*; SEG: Tulsa, OK, USA, 1986; p. 526.
51. Boganik, G.N.; Gurvich, I.I. *Seismic Exploration*; AIS: Tver, Russia, 2006; p. 744. (In Russian)
52. Miller, R.D.; Bradford, J.H.; Holliger, K. (Eds.) *Advances in Near-Surface Seismology and Ground-Penetrating Radar*; SEG Geophysical Developments Series No. 15; Society of Exploration Geophysicists; American Geophysical Union; Environmental and Engineering Geophysical Society: Tulsa, OK, USA; Washington, DC, USA, 2010; p. 487.
53. Bobachev, A.A.; Marchenko, M.N.; Modin, I.N.; Pervago, E.V.; Urusova, A.V.; Shevnin, V.A. Resistivity surveys in a horizontally heterogeneous earth: New approaches. *Izv. RAN Fiz. Zemli* **1995**, *12*, 79–90.
54. Stefanescu, S.; Schlumberger, C.; Schlumberger, M. Sur la Distribution Électrique Potentielle autour d'Une Prise de Terre Ponctuelle Dans un Terrain à Couches Horizontales Homogènes et Isotropes. *J. Phys. Radium* **1930**, *4*, 132–140. [[CrossRef](#)]
55. Khmelevskoy, V.K. *Resistivity Surveys. Student's Manual*; Moscow University: Moscow, Russia, 1984; p. 422. (In Russian)
56. Kalinin, A.V.; Khmelevskoy, V.K.; Vladov, M.L.; Zolotaya, L.A.; Kulnitsky, L.M.; Starovoitov, A.V.; Tokarev, M.Y.; Shalava, N.V. Modern georadar surveys. *Razved. Okhrana Nedr.* **2001**, *3*, 2–6.
57. Vladov, M.L.; Starovoitov, A.V. *Fundamentals of Ground Penetrating Radar Surveys*; Moscow University Press: Moscow, Russia, 2004; p. 155. (In Russian)
58. Finkelshtein, M.I.; Kutev, V.A.; Zolotarev, V.P. *Near-Surface Ground Penetrating Radar Surveys for Engineering Geology*; Nedra: Moscow, Russia, 1986. (In Russian)
59. Buddo, I.V.; Sharlov, M.; Shelokhov, I.; Misyurkeeva, N.; Seminsky, I.; Selyaev, V.; Agafonov, Y. Applicability of transient electromagnetic surveys to permafrost imaging in Arctic West Siberia. *Energies* **2022**, *15*, 1816. [[CrossRef](#)]
60. Kaufman, A.A.; Morozova, G.M. *Transient Electromagnetic Soundings: Theoretical Background*; Nauka: Novosibirsk, Russia, 1970; p. 123. (In Russian)
61. Tabarovskiy, L.A.; Eпов, M.I.; Sosunov, O.G. *Estimating the Resolution of Electromagnetic Surveys and Noise Attenuation*; IGI SO AN SSSR: Novosibirsk, Russia, 1985; p. 47. (In Russian)
62. Vanyan, L.L. *Electromagnetic Soundings*; Nauchny mir: Moscow, Russia, 1997; p. 218. (In Russian)
63. McNeill, J.D. *Application of Transient Electromagnetic Techniques*; Geonics Limited: Missasauga, ON, Canada, 1980; p. 17.
64. Korolkov, Y.S. *Transient Electromagnetic (TEM) Soundings for Petroleum Exploration*; Nedra: Moscow, Russia, 1987; p. 117. (In Russian)
65. Reynolds, J.M. *An Introduction to Applied and Environmental Geophysics*; John Wiley and Sons Ltd.: Chichester, UK, 1997; p. 796.
66. Mogilatov, V.S. *Induction Resistivity Surveys; Student's Manual*; Novosibirsk State University: Novosibirsk, Russia, 2014; p. 182. (In Russian)

67. Pospeev, A.V.; Buddo, I.V.; Agafonov, Y.A.; Sharlov, M.V.; Kompaniets, S.V.; Tokareva, O.V.; Misyurkeeva, N.V.; Gomylskiy, V.V.; Surov, L.V.; Ilyin, A.I. *Modern Resistivity Survey Practices*; GEO Publishers: Novosibirsk, Russia, 2018; p. 231. (In Russian)
68. Kozhevnikov, N.O.; Sharlov, M.V. Early-Time and Late-Time Limitations on the Performance of Near-Surface TEM Measuring Systems. In Proceedings of the Near Surface Geoscience Conference & Exhibition 2019, Hague, The Netherlands, 8–12 September 2019.
69. Sharlov, M.V.; Kozhevnikov, N.O.; Pesturina, T.N. Improving the performance of measurement systems for shallow TEM soundings. In Proceedings of the VIII Russian Seminar on Resistivity Surveys 2021., Moscow, Russia, 26 September–2 October 2021. (In Russian).
70. Sharlov, M.V.; Buddo, I.V.; Misyurkeeva, N.V.; Shelokhov, I.A.; Agafonov, Y.A. Transient electromagnetic surveys for high resolution near-surface exploration: Basics and case studies. *First Break* **2017**, *35*, 63–71. [[CrossRef](#)]
71. Available online: <http://zond-geo.com/software/resistivity-imaging-ves/zondres2d/> (accessed on 9 October 2022).
72. Agafonov, Y.A.; Pospeev, A.V.; Surov, L.V. Electromagnetic surveys in the southern Siberian craton: System for data interpretation and main uses of transient electromagnetic surveys. *Prib. I Sist. Razvedochnoi Geofiz.* **2006**, *1*, 33–36.
73. Misyurkeeva, N.; Buddo, I.; Shelokhov, I.; Smirnov, A.; Agafonov, Y.; Nezhdanov, A.; Tokareva, O. The structure of the permafrost section from high-density transient electromagnetic method (TEM) data within the Yamal Peninsula. In Proceedings of the ProGRESS'21 Conference, Sochi, Russia, 1–3 November 2021; pp. 1–6.
74. Rybalchenko, V.V.; Trusov, A.I.; Buddo, I.V.; Abramovich, A.V.; Smirnov, A.S.; Misyurkeeva, N.V.; Shelokhov, I.A.; Otsimik, A.A.; Agafonov, Y.A.; Gorlov, I.V.; et al. Additional studies in petroleum exploration and development: From permafrost mapping to groundwater prospecting for drilling and operation of wells. *Gazov. Promyshlennost* **2020**, *11*, 20–28.